Probing of Electronic and Optical Properties of Silver Halide Micro- and Nanocrystals by Cryo-EFTEM and EELS

Vladimir P. Oleshko

Department of Materials Science & Engineering, University of Virginia, Charlottesville, VA 22904, USA

Abstract

Due to an opportunity to probe valence electron excitations in solids caused by inelastic scattering with high spatial and spectral resolution, cryo-energy-filtering transmission electron microscopy (EFTEM) and electron energy-loss spectroscopy enable to characterize local electronic, dielectric and optical properties of individual composite AgBr core - Ag(Br,I) shell tabular micro-crystals (t-MCs) and uniform Ag(Br,I) nanocrystals (NCs). The complex dielectric permittivity, optical joint density of states, refractive index, extinction and absorption for t-MCs and NCs derived from experimental data via Kramers-Kronig relations have been compared with ab initio *LMTO-ASA calculations for AgBr. Contrast tuning with the selected energy window in the range 0-100 eV enables visualizing valence electron excitations in silver halides caused by interband transitions and Mott-Warnier excitons. The non-uniform contrast of NCs revealed by cryo-EFTEM was referred to predominant excitations at surfaces and near edges accompanied with a coupling of surface and volume losses. The size-confined coupling of surface and volume losses in the size range where deviations from bulk crystal selection rules occur could result in periodical oscillations of the image intensity with the NC size. A size-dependent enhancement of exciton-assisted* $\Gamma_{8^-}, \Gamma_{6^-} \rightarrow \Gamma_6$ *interband transitions at 4 eV correlates with the enhancement of free exciton luminescence from NCs when their size is less than 100 nm due to contributions to the energy-level structure from carrier confinement and surface states.*

Introduction

Silver halides, AgX (X=Br, I, Cl), well known as quantum detectors, exhibit many remarkable solid-state properties that have made them highly attractive both for fundamental and applied research. In addition to the unique character of optical absorption, the strong quadrupolar deformability of the Ag^+ is responsible for a soft crystal lattice, which is significantly less rigid than one for cations of alkali halides. Among these properties, there are also unusually small lattice constants, but large lattice energies and dielectric constants, peculiarities of elastic constants and phonon spectra, low solubility, predominance of Frenkel defects, high mobility of interstitials and dislocations, that have made silver halides useful in numerous applications (imaging and information recording systems, photonic and optical devices, etc.). The Ag 4d-states and the halogen p-states in AgX are close to each other, thus leading to considerable complexity in the valence-band structure. The occurrence of a low energy indirect gap between the valence and conduction bands results in size restriction effects on the electronic properties of nanocrystalline silver halides, when the particle size decreases below 100 nm [1-4]. Quantum confinement usually occurs when the spatial extent of a material (boundary conditions) begins to affect the eigenenergies of the electron wave function, causing the electronic properties to differ from those of bulk solid. Considering the relaxation properties of excitons in AgBr, quantum size effects may be expected for crystal sizes much larger than the Bohr radius of the indirect exciton ~3 nm. The restricted geometry leads to the occurrence of surface recombination that becomes a dominant relaxation channel in crystals with sizes already less than 500 nm [5]. Quantum effects of excitons in AgX nanocrystals (NCs) have been demonstrated by the appearance of the indirect exciton luminescence forbidden by selection rules in large crystals and by an increase of its quantum yield by several orders of magnitude when the particle size is decreased from 80 nm to 7.9 nm [6, 7]. A high-energy shift of luminescence band maxima of free excitons in the case of 40 nm-sized Ag(Br,I) NCs was also found [7, 8]. The position of the phonon-assisted emission lines was shifted by 1.8 meV to high energies and the zero-phonon emission was increased in intensity due to band restructuring induced by the size effect. The indirect excitonic luminescence was observed starting with crystals of 80 nm in cubic edge length on the same scale as the other emission bands and its intensity increased as size decreased [7, 9]. At edge lengths of 50 nm, the exciton emission is of the same order of magnitude as the other emission bands. The cause of this enhancement is thought to be due to the quantum size effect in conjunction with contribution of the spatial electron and hole confinement and diminishing iodide-bound exciton (IBE) emission [5, 9].

For better understanding photophysical properties of nano-crystalline silver halides, it is necessary to evaluate their electronic structure in the size range where deviations from the bulk crystal selection rules occur. Due to an opportunity to probe electron excitations caused by inelastic scattering with high spatial (0.1-1.0 nm) and spectral (0.1-1.5 eV) resolution, energy-filtering transmission electron microscopy and electron energy-loss spectroscopy (EFTEM/EELS) offer possibilities to explore photophysical properties of AgX nanocrystalline matter. Combined with quantum-mechanical calculations, this may provide copious information on the nanoscale band structure, density of states, bonding, dielectrical and optical parameters of silver halides. This paper reports on electronic and optical properties of individual high-aspect-ratio composite tabular Ag(Br,I) microcrystals (*t*-MCs) and uniform Ag(Br,I) NCs investigated by cryo-EFTEM/ EELS. The results have been compared with *ab initio* calculations for AgBr by a linear muffin-tin orbital method in its atomic spheres approximation (LMTO-ASA) that is shown to be capable of

describing the dielectric behavior of AgBr and exciton transition regions above the direct band gap at 4.3 eV [4].

Experimental

Uniform Ag(Br,I) NCs of 22-185 nm in diameter, containing 5 mol.% of AgI, and Ag (Br, I) nanostructured composite tabular microcrystals (*t*-MCs), 2-10 μm in size and 100-120 nm in thickness, containing 3-8 mol. % of AgI in the shells, were synthesized by a computer-assisted double jet method. Procedures of specimen preparation for microscopic studies were described elsewhere [10]. All preparations and handling were done under non-actinic light to avoid the formation of printout silver.

Microscopy and spectroscopy studies were performed using a unit composed of a ZEISS CEM 902 and a JEOL JEM 1200EX TEMSCAN-EDX analytical electron microscopes, both connected to a Kontron IBAS-2000 image analysis system. EFTEM and EELS measurements were made on the ZEISS CEM 902 computerized electron microscope operating at accelerating voltage 80 kV and equipped with an integrated energy filter. EFTEM images were acquired with an exit energy-selecting slit of 5-10 eV. EEL spectra were recorded with the illumination semiangle α of 2.5 mrad and the collection semiangle β varied from 6 to 35 mrad. The energy resolution was 1.2-1.5 eV, based on the measured FWHM of the zero-loss peak. Radiation damage of the specimens was essentially reduced using a top-entry cryo-stage at T=-193°C supplied with a modified evacuated cooling trap. A KONTRON IBAS-2000 image analysis system was utilized to control acquisition parameters on-line and to perform automatic on-line/off-line processing of data. After input of the dwell time per pixel, frame loops, total number of pixels, a window of analysis and position of energy window, the computer hardware took control over the scanning system–EDX (the JEM 1200EX) or over the acquisition and processing of spectroscopic images (the ZEISS CEM 902) [10].

Results and Discussion

EEL spectra of Ag(Br,I) *t*-MCs and NCs (Fig. 1) exhibit a low-loss fine structure assigned to interband transitions caused by mixing the Ag 4d states with the X 4p states at various points in the Brillouin zone (4-18 eV), a bulk plasmon (22-24 eV) and minor inner-shell excitations (55-70 eV) [1, 3, 7-9]. The spectra indicate a low energy shift of a proposed exciton peak at 15-17 eV and volume losses with decreasing the crystal size. Local excitations inside NCs corresponding to interband transitions and volume plasmon (VP) losses have been visualized using contrast tuning in the low-loss range (Fig. 1) since variations in EFTEM intensities follow EEL spectral intensity variations [10-13]. The image intensity changes lead to contrast reversal when the energy was tuned over the range. This allows visualizing an internal crystal structure since the Bragg contrast is preserved in inelastic scattering processes. At first, irradiating electrons hit the crystal directly causing internal ionization with the generation of electron-hole pairs. Swift electrons may also not strike the particle directly, but cause polarization inside it by their Coulomb field. Polarization waves formed by Mott-Wannier excitons are a prominent type of electronic excitation for AgBr [14]. Iodine in AgBr acts as an isoelectronic trap for holes at low temperatures, producing a positively charged center. The latter can be neutralized by binding an electron, thus forming the IBE [15]. Selection of proposed exciton losses at E = 16 eV (Fig. 1, inset) resulted in a weak rim around NCs, because such losses can extend at distances of a few nanometer away from the particle that corresponds satisfactorily to the expected exciton size for AgX (X=I, Br) [1]. No rims were found in the zero-loss mode (see the profile across the same NC). A lateral distribution

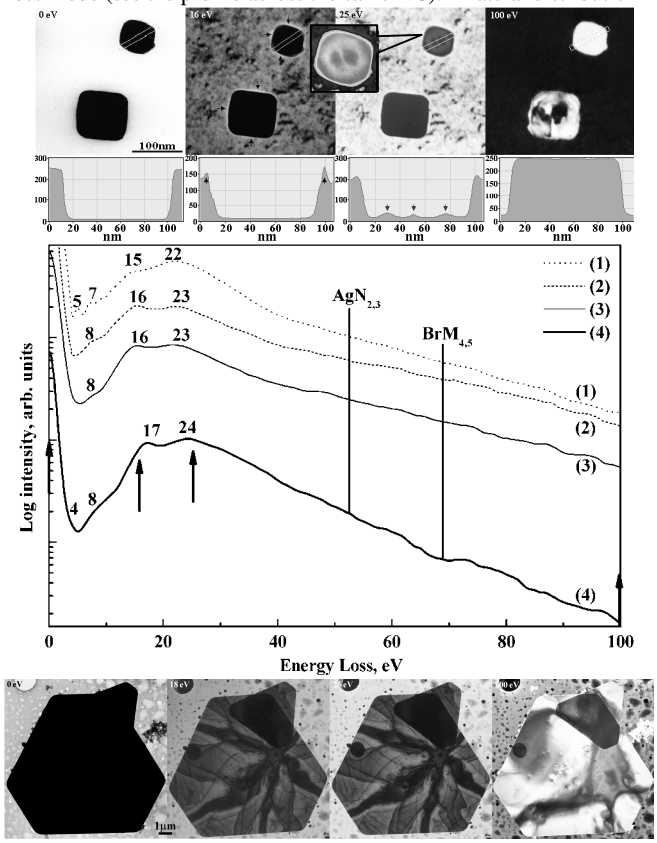

***Figure 1**. Cryo-EFTEM (at selected energy losses, large bold up arrows) and EELS of Ag(Br,I) NCs and t-MCs, t=-177°C: NCs (upper row) and t-MCs (bottom row). Graphs show intensity profiles across the right NC as marked by rectangular boxes, a 30 pixel integration width. Small up arrows point to exciton states observed at 16 eV, small down arrows indicate periodical oscillations due to size confined coupling of SP and VP excitations at 25 eV. An enlarged inset demonstrates the lateral distribution of VPs confined within a θ-like volume inside NC. (1) NC, 50±4 nm nm; (2) NC, 109 ±7 nm; (3) T-MC, AgBr core, 100±20 nm thick; (4) T-MC, Ag(Br,I) shell, 120±20 nm thick.*

of VPs created inside the NC is visualized by positioning the energy window at E = 25 eV. With essentially decreased background at E = 100 eV, minor inner-shell excitations and tales of surface (SP) and VP excitations are observed with the contrast reversal. The non-uniform contrast inside the NCs is referred to predominant excitations at the surfaces and near the edges; this can decrease the probability of VP losses because of the sum rule [16]. When the fields due to SP losses reach throughout the structure, they couple and the probability for their generation becomes periodic in the size of the system [16, 17]. Numerical calculations of the VP loss probability reveal its damped oscillations as a function of the nanoparticle radius [18]. Both plasmons and excitons are considered to be coherent superposition of electron-hole excitations corresponding to transitions from occupied to unoccupied states [19]. Since electronic sum rules must be satisfied for each i th excited Ag^+ and X^- ion (i= 1, 2, $N \approx 2.3 \times 10^4$) [10, 13]:

$$\sum_{i=1}^{i=N} \int \frac{df}{dE} dE = \sum_{i=1}^{i=N} z_i = \sum_{j=1}^{j=N_{sp}} z_j + \sum_{l=1}^{l=N_{vp}} z_l \qquad (1)$$

Here the first term is the sum of integrals of a generalized oscillator strength per unit energy loss over selected energy loss E, df/dE, which governs a differential cross-section or scattered intensity. It is constrained by the number of valence electrons (10 4d electrons (Ag^+) and 6 4p (5p) electrons (Br^-, I^-) per AgX unit), involved in excitations within a confined NC volume, $\sum_{i=1}^{i=N} z_i$, where z_i is the number of electrons in a ith ion, and $N=N_{sp}+N_{vp}$ is the sum of ions contributing to SP and VP, respectively. With increasing N_{sp}, SP excitations necessarily reduce the strength of bulk excitations. Consequently, VP losses should exhibit similar periodic behavior. Coupling of the losses can then cause oscillations of their intensities with the particle size and induced charge (Fig. 1, the profile across the NC at 25 eV) due to contributions to the energy-level structure from carrier confinement and surface states. Areas of the reduced VP loss intensity are confined within a 5 nm-thick surface layer and also appear inside the NC as two symmetrical regions of 5nm x 10 nm in size surrounded by a -like region of the increased VP loss intensity.

Kramers-Kronig analysis (KKA) has been employed to calculate the energy dependence of dielectric permittivity. In principle, the KKA should be carried out for known momentum transfer between initial and final states. However, it is possible to obtain ε_1 and ε_2 for transitions confined to small momentum transfers only through KK transformation. Since $Im\ (-1/\varepsilon)$ is overwhelmed by the zero-loss peak, the KKA appears to be sensitive to the intensity inputs at the low-energy end. This could introduce uncertainties at energies below 3 eV. To overcome the problem, a smooth extrapolation of the intensities to zero energy was applied [10]. For each EEL spectrum, contributions from the zero-loss peak and due to multiple losses have been subtracted and corrections for the angular weighting were made. Figs. 2a and 2b present the KK-derived energy-loss function, $1/\varepsilon$, and dielectric permittivity, $\varepsilon=\varepsilon_1+i\varepsilon_2$, for Ag(Br,I) NCs (***1***) and (***2***), a non-confined composite *t*-MC (AgBr core,) of the same thickness as NCs (***2***) [11] and *ab initio* LMTO-ASA calculations for AgBr [4], respectively. Experimental curves fall to 0 at $E<3$ eV taking into account the indirect exciton band gap, E^i_g, at 2.68 eV. For low energy losses $E\leq\hbar\omega_p$ =21.6 eV, the energy-loss function,

$$Im\ (-1/\varepsilon) = \frac{\varepsilon_2}{\varepsilon_1^2+\varepsilon_2^2} = \frac{\omega\Gamma\omega_p^2}{(\omega^2-\omega_p^2)^2+(\omega\Gamma)^2}, \qquad (2)$$

describes many-electron excitations against the ionic background caused by oscillations of bound electrons and exciton-assisted interband transitions [13]. Here Γ is the damping constant; ω_p is the plasma resonance frequency. The energy of the VP resonance was estimated as $\hbar\omega_p=[(\hbar\omega_p^f)^2+E^{i}_{g}{}^2]^{1/2}$=21.6 eV, where $\hbar\omega_p^f=\hbar[ne^2/(\varepsilon_0 m)]^{1/2}$=21.4 eV, ω_p^f=3.3x10^{16} Hz is the free electron plasma frequency, n is the electron density, e is the electron charge, ε_0 is the permittivity of vacuum, and m is the electron mass. So, the calculated $\hbar\omega_p$ appeared to be close to the experimental value with the accuracy of measurements.

When ε_1 has a local minimum (this points to the instability of the system against external perturbations leading to excitations) and ε_2 is small (this indicates small damping of oscillations due to absorption), $Im\ (-1/\varepsilon)$ exhibits maxima corresponding to interband transitions at 5, 7, 15-17 eV and VP at 22 eV (Fig. 2a). ε_1 describes the polarizability of the specimen with local minima at 5, 8, 12-15 eV and 21 eV, while ε_2 is related to absorption with local maxima at 4, 7-8, 10, and 15-17 eV (Fig. 2b). ε_1 and ε_2 are connected by integral KK relationships because of causality being involved in dielectric response. Self-consistent LMTO-ASA calculations of dielectric parameters for AgBr have been performed assuming that all transition matrix ($|M|$) elements are equal and independent of the k-point and the band number of the initial (j) and final (j') electron states, $\vec{k}=\vec{k}_{j}=\vec{k}_{j'}$. The following expressions for ε_1 and ε_2 have been derived [4]:

$$\varepsilon_1=1+\frac{V_1\hbar^2}{\pi}\sum P\int_{BZ}\frac{1}{[E_{j'}(\vec{k})-[E_j(\vec{k})]^2[E_{j'}(\vec{k})-E_j(\vec{k})-\hbar\omega]}d^3k \qquad (3)$$

$$\varepsilon_2=\frac{V_2}{\omega^2}\sum_{jj'}\int_{BZ}\delta(E_{j'}(\vec{k})-E_j(\vec{k})-\hbar\omega)d^3k \qquad (4)$$

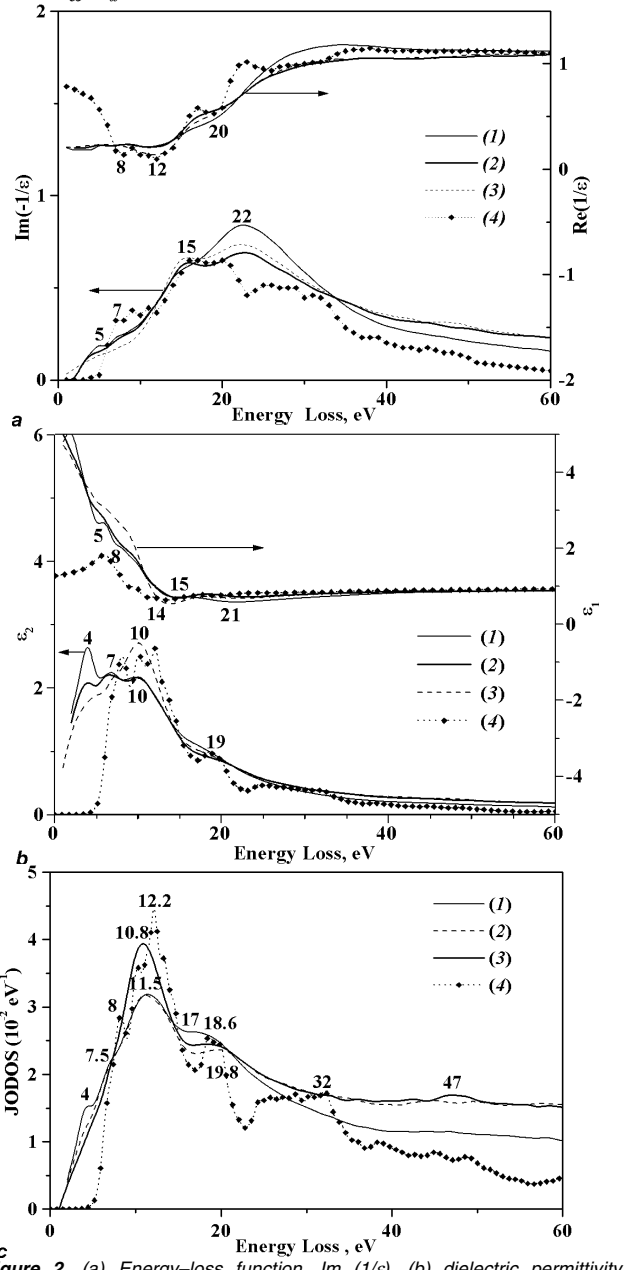

Figure 2*. (a) Energy–loss function, Im (1/ε), (b) dielectric permittivity, $\varepsilon=\varepsilon_1+i\varepsilon_2$, and (c) joint optical density of states (OJDOS), $J_1(E)=E\varepsilon_2/0.5\pi E_p^2$, for Ag(Br,I) NCs (**1**) and (**2**) with mean equivalent diameters of 50±4 nm (1), and of 109±7 nm (2), a t-MC (AgBr core, 102±20 nm thickness) (3)) and ab initio LMTO-ASA calculations for AgBr (4), respectively.*

Here P denotes the principal value of the integral and fitting parameters $V_1=\frac{2h^2e^2}{\pi^2m^2}|M|^2$ =0.04 and $V_2=\frac{2h^2e^2}{\pi n^2\varpi^2}|M|^2$ =0.01, respectively. The needed energies $E_{j(j')}(\bar{k})$ have been taken from the LMTO-ASA energy band calculations for AgBr [4]. Although calculated ε_2 and *Im* (*-1/ε*) fall to zero at 4.3 eV due to limitations of the model, the maxima of ε_2 at 8 eV, 10 eV and 12 eV satisfactorily fit to the composite band at 7-14 eV (with maxima at 8 eV and 10 eV) assigned to the direct band-to-band and exciton assisted transitions at X point (unresolved $(X_6^-, X_6^-, X_7^-)\rightarrow X_6^+$) [4, 20]. The minimum of computed ε_1 at 12 eV fits well to the minimum of experimental ε_1 curves, similarly to the minimum of *Re* (*1/ε*) at 12 eV as well as of the minimum of ε_1 at 21 eV, where *Im* (*-1/ε*) has its maximum. The crossings of *Re* (*1/ε*) and *Im* (*-1/ε*) at about 7 eV coincide. The shoulder of ε_2 starting at 15-17 eV superimposed with the previous band and the corresponding maximum of *Im* (*1/ε*) was referred to excitonic transitions with Γ_6^+ symmetry. In spite of obvious similarities, ε_1 and ε_2 exhibit size variations. So, ε_2 shows reverse-order changes in relative intensities of the bands for NCs (***1***) comparatively to NCs (***2***) and a *t*-MC (Fig. 2b), i.e., the increased intensity of the band at 4 eV (unresolved direct exciton transitions involving the spin-orbit split valence and conduction band states at Γ point, $(\Gamma_8^-, \Gamma_6^- \rightarrow \Gamma_6^+)$[14, 20]), relatively to the bands at 7 eV and 10 eV ($(X_6^-, X_6^-, X_7^-)\rightarrow X_6^+$) transitions at X point) [1, 6]. This correlates with a quantum confined enhancement of free exciton luminescence from AgBr NCs below 80 nm [1, 2, 7, 9]. The differences in ε between NCs (***1***) and AgBr *t*-MC cannot be referred to IBEs because of a low content of iodide in individual NCs, 2-3 at% [10]. The intensities of ε_2 bands at 8 eV and 10 eV for an iodide-enriched Ag(Br,I) shell of the same *t*-MC appear to be further increased as compared to a AgBr core that is likely due to IBEs [11, 12].

The optical joint density of states (OJDOS), $J_1(E) = \varepsilon_2/0.5\pi E_p^2$, (Fig. 2c) demonstrates an increasing confinement of the s- and p-DOS at 4 eV (1st conduction band) and of the mixed DOS above 7.5 eV (2nd conduction band) with the crystal size due to the band restructuring induced by the restricted size, followed a decrease in the DOS at 10.8-12.2 eV as compared to non-confined NCs (***2***) and *t*-MC and *ab initio* LMTO-ASA calculations [4, 21].

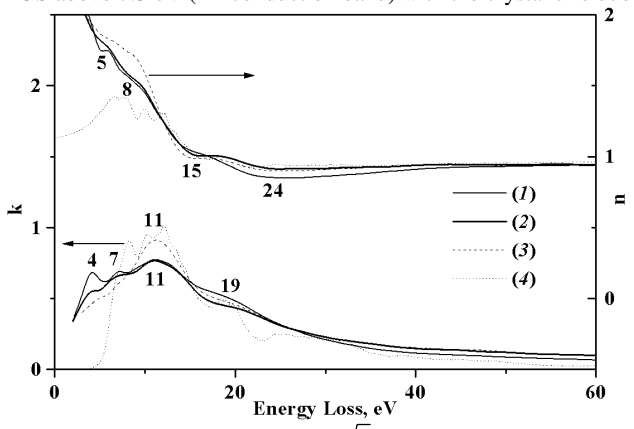

Figure 3. *Complex refractive index, $N=\sqrt{\varepsilon}=n+ik$, for Ag(Br,I) NCs with the mean equivalent diameter of 50±4 nm (**1**) and 109±7 nm (**2**) in comparison with a AgBr t-MC of 102±20 nm in thickness (**3**) and ab initio LMTO-ASA calculations for AgBr (**4**). Curves fall to 0 at E<3 eV taking into account the indirect band gap, E_g', at 2.68 eV.*

Fig. 3 presents experimental and calculated curves for the KK-derived complex refractive index, $N=\sqrt{\varepsilon}=n+ik$. Here the index of refraction, $n=\{0.5[(\varepsilon_1^2+\varepsilon_2^2)^{0.5}+\varepsilon_1]\}^{0.5}$, and the extinction coefficient, $k=\{0.5[(\varepsilon_1^2+\varepsilon_2^2)^{0.5}-\varepsilon_1]\}^{0.5}$ are given. The values of n closely approach 1.0 above 15 eV. For NCs (***1***) (Fig. 3), the imaginary part of refractive index (extinction coefficient), k, again exhibits an enhanced intensity of the direct exciton transition at Γ point (the band at 4 eV) relatively to transitions at X point (the bands at 7 eV and 11 eV, respectively). The absorption coefficient, $\mu = 2Ek/\hbar c = E/(\hbar c)[2(\varepsilon_1^2+\varepsilon_2^2)-2\varepsilon_1]^{0.5}$ essentially follows the OJDOS because $k = \varepsilon_2/2n$ [21].

Acknowledgement

The work was supported in part by the US Department of Energy, under contract DE-FG02-01ER45918.

References

[1] A. P. Marchetti, R. P. Johansson and G. L. McLendon, Phys. Rev. B 47, 4268 (1993).

[2] M. I. Freedhoff, A. P. Marchetti and G. L. McLendon, J. Luminesc. 70, 400 (1996).

[3] P. J. Rodney, A. P. Marchetti and P. M. Fauchet, Phys. Rev. B 62(7), 4215 (2000).

[4] V. Oleshko, M. Amkreutz and H. Overhof, Phys. Rev. B 67**,** 115409-1 (2003).

[5] M. Timme, E. Schreiber, H. Stolz and W. von der Osten, J. Luminesc. 55, 79-86 (1993).

[6] H. Kanzaki and Y. Tadekuma, Solid. State Comm. 80, 33 (1991).

[7] K. P. Johansson, A. P. Marchetti and G. L. McLendon, J. Phys. Chem. 96, 2873 (1992).

[8] U. Scholle, H. Stolz and W. von der Osten, Solid State Comm. 86, 657 (1993).

[9] K. P. Johansson, G. McLendon and A. Marchetti, Chem. Phys. Lett. 179 (4), 321 (1991),

[10] V. P. Oleshko**,** A. Van Daele, R. H. Gijbels and W. A. Jacob, Nanostruct. Mater. 10(8), 1225 (1998); ibid 11(5), 687 (1999).

[11] V. P. Oleshko, R. H. Gijbels, W. A. Jacob, Micron 31, 55 (2000).

[12] V. P. Oleshko, in *Industrial Applications of Electron Microscopy,* edited by Z. R. Li, (M. Dekker, N. Y., 2002), pg. 51-112.

[13] R. F. Egerton, *Electron Energy-Loss Spectroscopy in the Electron Microscope*, 2nd ed., (Plenum Press, N. Y., 1996), pg. 151, 256, 414.

[14] N. J. Carrera and F. C. Brown, Phys. Rev. B 4, 3651 (1971).

[15] W. Czaja and A. Baldereschi, J. Phys. C. 12, 405 (1979).

[16] L. Reimer, in *Energy-Filtering Transmission Electron Microscopy*. (Springer-Verlag, Berlin, 1995) pg. 370-373.

[17] P. E. Batson, Surf. Sci. 156, 720 (1985).

[18] D. B. T. Thoai and E. Zeitler, Phys. Stat. Sol. (a) 107, 791 (1988).

[19] P. Schattschneider, B. Jouffrey, in Energy-Filtering Transmission Electron Microscopy. (Springer-Verlag, Berlin, 1995), pg.151-224.

[20] F. Bassani, R.S. Knox, W.B. Fowler, Phys. Rev. A 4, 1217 (1965).

[21] V. P. Oleshko, Microsc. Microanal. 11 (Suppl 2), 1462 (2005).

Author Biography

Vladimir Oleshko received his BS (1974), MS (1976) in Chemistry and PhD (1983) in Physical Chemistry from Moscow University. His research has focused on chemical physics and structural characterization of imaging materials. He is author of 139 publications and 76 presentations at scientific congresses and served as guest Editor for the topical issue of "*Microscopic Research of Silver Halides and Related Dispersed Systems*", Journal *Microscopy Research and Technique*, 42, 1998, member of IS&T since 1996.